J Mater Sci (2007) 42:7433–7445
DOI 10.1007/s10853-007-1583-0

Interlocking hexagons model for auxetic behaviour

N. Ravirala · A. Alderson · K. L. Alderson

Received: 16 November 2006 / Accepted: 6 February 2007 / Published online: 18 May 2007

Abstract A 2D 'Rough Particle' model consisting of interlocking hexagons is reported. Analytical expressions for the in-plane Poisson's ratios and Young's moduli due to particle translation along the geometrically matched male and female interlocks are derived for the model. The dependency of the mechanical properties on each of the model (geometrical and stiffness) parameters is provided, and it is shown that the assembly of interlocking hexagons deforming by particle translation along the interlocks displays auxetic (negative Poisson's ratio) behaviour. The model predictions are compared with experimental mechanical properties for auxetic polypropylene (PP) films and fibres. The model predicts the experimental Poisson's ratio values very well (model: ν_{xy} = –1.30, ν_{yx} = –0.77; experiment (PP films): $\nu_{\parallel}$ = –1.12, $\nu_{\perp} = -0.77$). The model generally overestimates the Young's moduli of the films, but is in reasonable agreement with the axial Young's modulus of the fibres.

Introduction

Auxetic materials when stretched axially expand instead of contracting laterally. Under axial compression, auxetic materials contract laterally. In other words, auxetic materials exhibit negative Poisson's ratio behaviour [1]. A variety of auxetic materials and structures have been fabricated, including honeycombs [2], polymeric and metallic foams [3], and microporous polymers [4, 5]. Naturally occurring auxetic materials exist, including biomaterials [6] and molecular-level materials such as crystalline silica [7]. Auxetic materials can have enhanced properties over their conventional counter parts. For example, it has been shown experimentally that the indentation resistance [8] of auxetic materials has been enhanced by up to four times when compared with their conventional equivalent. Other enhanced properties include plane strain fracture toughness [9], energy absorption [10], and shear modulus [11].

Auxetic polymers

The first synthetic auxetic microporous polymer was an expanded form of polytetrafluoroethylene (PTFE) tape [12]. Subsequently, cylinders [13] (typically 1–2 cm in diameter and a few cm in length) of auxetic ultra high molecular weight polyethylene (UHMWPE) [4], polypropylene (PP) [5] and nylon [14] have been produced. It was found that the auxetic effect in these particular microporous polymers is strain-dependent and arises due to cooperative action of a complex microstructure [12] consisting of nodules of polymer interconnected by fibrils.

More recently, the production of auxetic PP fibres using a continuous partial melt extrusion process has been reported [15]. The partial melt extrusion process has now been developed to enable the continuous production of auxetic polyamide [16] and polyester [17] fibres, and also auxetic PP in film form [18]. The fibres have diameters in the range of 140–1,000 μm, and the film thickness is ~150 μm. Potential applications for auxetic fibres and films include as energy absorbing constituents in fibre-reinforced composites [19], anchoring devices [20], biomedical applications [21] and controlled delivery media [22], where active agents are entrapped and/or released from within

N. Ravirala · A. Alderson (✉) · K. L. Alderson
Centre for Materials Research and Innovation, The University of Bolton, Deane Rd, Bolton BL3 5AB, UK
e-mail: a.alderson@bolton.ac.uk

fibre/film micropores in response to an external stress stimulus.

The processing route for auxetic fibres and films comprises the compaction, partial (surface) melting and extrusion of polymer powder particles having an initially rough morphology and size distribution [15]. Experimental microscopy of the fibre/film microstructure indicates significantly lower levels of porosity and fibrillation than observed in the microstructure of the larger cross-section auxetic polymer cylinders. Rather, the fibre/film microstructure appears to resemble that of contacting or fused particles. This is shown in Fig. 1 where a cross-section of a 300 μm diameter auxetic PP fibre (micrograph taken perpendicular to the fibre axis) is presented [23]. To date no detailed model has been developed to describe the mechanism giving rise to auxetic behaviour in the auxetic fibres and films produced using the partial melt extrusion process.

Structures and mechanisms for auxetic materials

An idealised geometrical model of a regular array of rectangular nodules connected at their corners by fibrils was able to reproduce well the strain-dependent auxetic effect of the microporororous polymer cylinders and tapes. The auxetic effect was found to be due primarily to nodule translation arising from rotation of the fibrils under an applied load [24, 25].

For materials of lower porosity than that present in the microporous polymer cylinders, negative Poisson's ratios have been predicted for bonded granular materials where the particles are considered to interact by tangential (shear) forces as well as normal contact forces [26]. In the approach employed in Ref. [26], auxetic behaviour occurs when the tangential stiffness exceeds the normal contact stiffness. Such an occurrence may be achieved for granular assemblies comprising of contacting particles having a rough morphology.

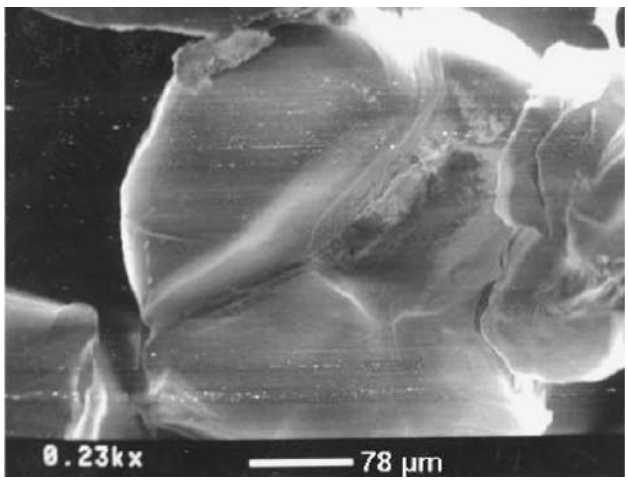

Fig. 1 SEM micrograph of a cross-section of auxetic PP fibre (diameter ~300 μm) [23]

Computer simulations of 2D rough disc assemblies have been performed [27]. In Ref. [27] the circumference of each rough disc consists of a number of small hard discs to form a 'hard cyclic multimer'. The simulations employed a hard body interaction potential and considered only nearest neighbour interactions between discs of different multimers. The Poisson's ratios of the hard cyclic multimer assemblies investigated were found to be dependent on the roughness of the multimer particles, which could be varied by varying the number of small hard discs per multimer. Auxetic behaviour was predicted when the 'roughness parameter' was sufficiently large.

The hard cyclic multimer model is an example of a number of modelling studies [28–34] that have been performed to understand mechanisms for auxetic behaviour at the molecular scale. At the macroscale, auxetic behaviour has been engineered in the horizontal plane of radially keyed graphite brick structures deployed in some nuclear reactor cores [35, 36]. The structures typically consist of free-standing columns of graphite bricks laterally connected by loose side and/or corner keys in keyways. The graphite bricks have square or hexagonal shapes in the horizontal plane, depending on the type of reactor core design. In effect, the key–keyway combinations produce a rough macroparticle assembly in which the 'particle' interactions are characterised by having tangential stiffness exceeding the normal contact stiffness. The keyed-brick structures expand in all radial directions when subjected to a tensile load in the horizontal plane by translation of the bricks through sliding of the bricks and radial keys along the rectangular keyways.

In this paper we report the development of an analytical rough particle model to predict auxetic behaviour. The model is developed to be consistent with the microscale features of the structure believed to give rise to auxetic behaviour in auxetic extruded polymer fibres and films. The essential features of the developed model should, therefore, be to realise auxetic behaviour from a microstructure having a particulate/granular nature and low porosity. The geometry of the model is derived from the geometry of the horizontal plane of the macroscale keyed-brick structure. For the purposes of ease of model development, this system has the attraction of having a single-mode deformation mechanism (particle translation), whereas in the alternative multimer systems the curved contacts between adjacent particles will lead to particle rotation and translation and therefore a more complex concurrent multiple mode deformation mechanism. The model predictions are compared with the experimentally measured mechanical properties of auxetic PP films and fibres.

Interlocking hexagon model

Model geometry

Figure 2 shows a schematic of the interlocking rough particle assembly comprising an array of rigid hexagonal particles connected through geometrically matched rectangular male–female interlock combinations located on adjoining edges of adjacent particles. Each hexagon has edge lengths l_1 and l_2. The edges of length l_1 are aligned parallel to the x axis, and the edges of length l_2 are at an angle α to the x axis, as shown in Fig. 2. The structure of interlocking regular hexagons ($l_1 = l_2$, $\alpha = 60°$) is analogous to that of the transverse plane of the graphite moderator core structure employed in the Tokai nuclear reactor [35].

Analytical expressions for the Poisson's ratios and Young's moduli due to particle translation as a result of sliding along the male–female interlock combinations are derived in the following.

Poisson's ratios

The unit-cell length, X, in the x-direction is given by,

$$X = 2(l_1 + l_2 \cos\alpha + a) \tag{1}$$

where a is a parameter defining the gap between adjacent hexagon particles, as defined in Fig. 2. The unit-cell length, Y, in the y-direction is given by,

$$Y = 2(l_2 \sin\alpha + a\cot\alpha) \tag{2}$$

For deformation of the structure by particle translation, the variable parameter is the gap parameter, a. The changes in the unit-cell lengths during deformation are determined by differentiating Equations (1) and (2) with respect to a:

$$\frac{dX}{da} = 2 \tag{3}$$

$$\frac{dY}{da} = 2\cot\alpha \tag{4}$$

The Poisson's ratio for loading in the x-direction is then given by,

$$v_{xy} = -\frac{d\varepsilon_y}{d\varepsilon_x} = -\frac{dY/Y}{dX/X} = -\left(\frac{dY}{da}\right)\left(\frac{dX}{da}\right)^{-1}\left(\frac{X}{Y}\right) \tag{5}$$

which is applicable to both linear and non-linear elastic deformation [37, 38]. Substituting Eqs. 1–4 into Eq. 5 gives

$$v_{xy} = -\frac{\cos\alpha(l_1 + l_2\cos\alpha + a)}{l_2\sin^2\alpha + a\cos\alpha} \tag{6}$$

Similarly, for loading in the y-direction,

$$v_{yx} = -\frac{l_2\sin^2\alpha + a\cos\alpha}{\cos\alpha(l_1 + l_2\cos\alpha + a)} = (v_{xy})^{-1} \tag{7}$$

Young's moduli

To derive expressions for the Young's moduli the conservation of energy approach is adopted [33, 39]. It is assumed each male–female interlock combination is connected by a spring of stiffness k_h (Fig. 3).

The work done per interlock, W_i, due to a change in the interlock gap perpendicular to the adjoining hexagonal faces, b_i, to $b_i + db_i$ is given by,

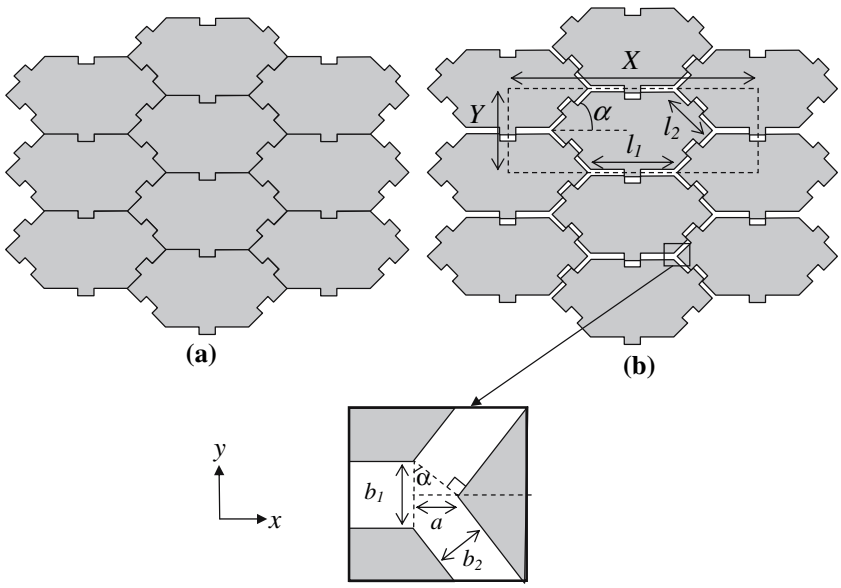

Fig. 2 Interlocking hexagon structure: (**a**) fully densified; (**b**) partially expanded

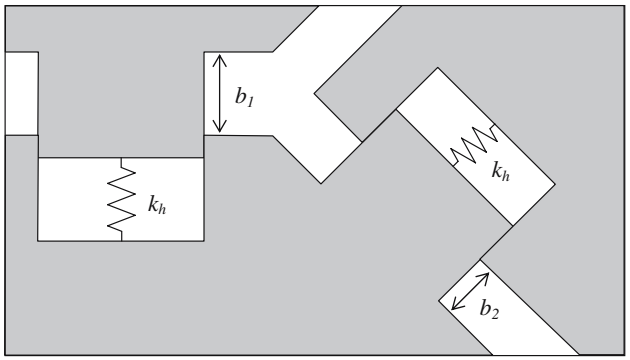

Fig. 3 Interlock combination connected by a spring

$$W_i = \frac{1}{2}k_h(db_i)^2 \tag{8}$$

The work done per unit cell (W_1) due to a change in b_1 to $b_1 + db_1$ for the interlock combinations associated with the sides of length l_1, assuming 1 interlock per adjoining interface (i.e. there are 2 of these interlocks per unit cell—Fig. 2), is therefore

$$W_1 = 2\left(\frac{1}{2}k_h(db_1)^2\right) \tag{9}$$

Now from Fig. 2,

$$b_1 = 2a\cot\alpha \tag{10}$$

giving

$$\frac{db_1}{da} = 2\cot\alpha \tag{11}$$

Similarly, the work done per unit cell (W_2) due to a change in b_2 to $b_2 + db_2$ for the interlock combinations associated with the sides of length l_2, assuming 1 interlock per adjoining interface (i.e. there are 4 of these interlocks per unit cell—Fig. 2), is

$$W_2 = 4\left(\frac{1}{2}k_h(db_2)^2\right) \tag{12}$$

Now again from Fig. 2,

$$b_2 = a\csc\alpha \tag{13}$$

$$\frac{db_2}{da} = \csc\alpha \tag{14}$$

The total work done per unit cell is given by,

$$W = W_1 + W_2 \tag{15}$$

Using Eqs. 9, 11, 12, 14 and 15, we get,

$$W = \left(\frac{1}{2}k_h(da)^2\right)(8\cot^2\alpha + 4\csc^2\alpha) \tag{16}$$

Now, the strain energy per unit volume for loading in the x-direction is given by,

$$U = \frac{1}{2}E_x(d\varepsilon_x)^2 = \frac{1}{2}E_x\left(\frac{dX}{X}\right)^2 = \frac{1}{2}E_x\left(\frac{1}{X}\frac{dX}{da}\right)^2(da)^2 \tag{17}$$

From the principle of conservation of energy,

$$U = \frac{W}{V} \tag{18}$$

where V is the volume of the unit cell.

Considering unit thickness in the z-direction,

$$V = XY \tag{19}$$

From Eqs. 16–19, we get

$$E_x = 4k_h\left(\frac{2\cos^2\alpha + 1}{\sin^2\alpha}\right)\left(\frac{X}{Y}\right)\left(\frac{dX}{da}\right)^{-2} \tag{20}$$

Substituting Eqs. 1–3 into Eq. 20:

$$E_x = k_h\left(\frac{2\cos^2\alpha + 1}{\sin\alpha}\right)\left(\frac{l_1 + l_2\cos\alpha + a}{l_2\sin^2\alpha + a\cos\alpha}\right) \tag{21}$$

Using a similar approach for loading in the y-direction, it can be shown that

$$E_y = k_h\left(\frac{2\cos^2\alpha + 1}{\sin\alpha\cos^2\alpha}\right)\left(\frac{l_2\sin^2\alpha + a\cos\alpha}{l_1 + l_2\cos\alpha + a}\right) \tag{22}$$

Note that, whereas the expressions for Poisson's ratio (Eqs. 6 and 7) contain purely geometrical terms, the expressions for Young's modulus (Eqs. 21 and 22) contain the spring stiffness constant in addition to the geometrical model parameters.

According to classical elasticity theory, thermodynamic considerations require a material to have a symmetric compliance matrix [40], i.e.

$$\nu_{xy}E_y = \nu_{yx}E_x \tag{23}$$

From Eqs. 6, 7, 21 and 22

$$\nu_{xy}E_y = \nu_{yx}E_x = -k_h\left(\frac{2\cos^2\alpha + 1}{\sin\alpha\cos\alpha}\right) \tag{24}$$

thus satisfying the requirement of a symmetric compliance matrix.

Also it is noted that for the case of the regular close packed interlocking hexagon structure ($\alpha = 60°$ and $l_1 = l_2$), $E_x = E_y$ and $v_{xy} = v_{yx} = -1$. The regular close packed interlocking hexagon structure is, therefore, isotropic as expected from symmetry.

Particle aspect ratio

In order to facilitate comparison with experiment it is necessary to derive an expression for the aspect ratio of the interlocking particles which can then be related to the aspect ratio of the fused/contacting particles in the fibres and films. For the purposes of this work, the model aspect ratio is defined by the aspect ratio of the ellipse inscribed within the hexagon (Fig. 4).

The aspect ratio of an ellipse inscribed within a hexagonal cell is (see Appendix)

$$\frac{A}{B} = \frac{1}{2l_2 \sin\alpha}\sqrt{l_1^2 + 4l_1 l_2 \cos\alpha} \tag{25}$$

where A and B are the axes of the ellipse aligned along the x and y directions, respectively.

Results—parametric study

In order to consider the effect of each of the structural parameters (l_1, l_2, a and α) on the Poisson's ratios and Young's moduli for the interlocking hexagon structure we first define a 'standard' parameter set: $\alpha = 60°$ and $l_1 = l_2 = 1$ arbitrary units, corresponding to the regular hexagon. A 'standard' gap parameter is arbitrarily chosen to be 1% of the edge length values, i.e. $a = 0.01$ arbitrary units. In the following, each geometrical parameter is varied in turn while maintaining the other structural parameters equal to the standard value.

Poisson's ratio trends

Figure 5 shows the Poisson's ratio dependency on the hexagon angle α. The Poisson's ratios are negative in the range $0 \leq \alpha < 90°$. As α increases in the range $0 \leq \alpha \leq 90°$, the magnitude of v_{xy} decreases from an infinitely negative value at $\alpha = 0°$ to $v_{xy} = 0$ when $\alpha = 90°$. For α in the range $90 < \alpha \leq 120°$, the hexagons have a re-entrant shape (Fig. 6), and the Poisson's ratio (v_{xy}) is positive. Re-entrant hexagons with $120 < \alpha \leq 180°$ are not possible when $l_1 = l_2$. The dependency of v_{yx} on α is the reciprocal of the v_{xy} behaviour, tending towards infinitely large values as $\alpha \rightarrow 90°$.

The dependency of Poisson's ratio on the side length l_1 is shown in Fig. 7. For the standard parameter set employed in this study, the Poisson's ratios are always negative for all values of $l_1 > 0$ (l_1 cannot be less than zero for the 2D model of rigid hexagons). $v_{xy} = -0.34$ when $l_1 = 0$ (corresponding to rigid interlocking diamond-shaped particles), and increases linearly in magnitude with increasing l_1. $v_{yx} = -2.96$ when $l_1 = 0$ and decreases in magnitude in a non-linear manner with increasing l_1, tending to zero as $l_1 \rightarrow \infty$.

Both Poisson's ratios have a non-linear dependency on l_2 (Fig. 8). As the value of l_2 increases the magnitude of v_{xy} decreases from a large (but finite) value at $l_2 \sim 0$ to $v_{xy} = -0.33$ as $l_2 \rightarrow \infty$. Conversely, v_{yx} increases from a small ($v_{yx} \sim -0.01$) value at $l_2 \sim 0$ to $v_{yx} = -3$ as $l_2 \rightarrow \infty$.

v_{xy} and v_{yx} both equal –1 for the standard parameter set of $\alpha = 60°$ and $l_1 = l_2 = 1$, irrespective of the value of a (Eqs. 6 and 7). However, for non-standard parameter sets the values of Poisson's ratios are dependent on the value of a. For example, Fig. 9 shows the Poisson's ratio variations with respect to a when $\alpha = 30°$, $l_1 = 2$ and $l_2 = 0.5$. For this parameter set the Poisson's ratios have near-linear dependencies over the range of a considered in Fig. 9: v_{xy}

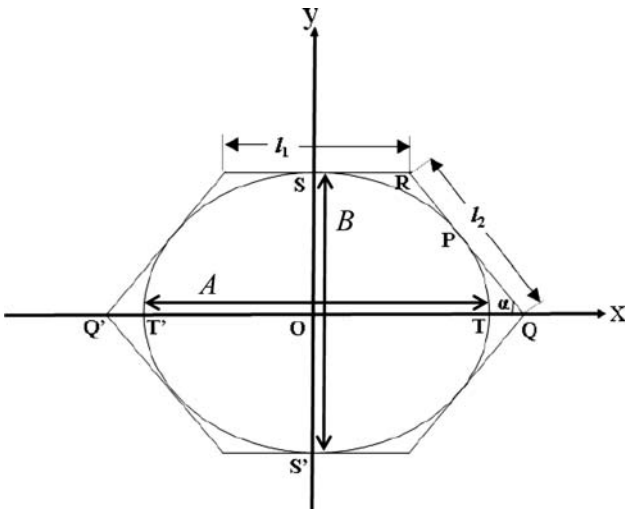

Fig. 4 Inscribed ellipse of a non-regular hexagon

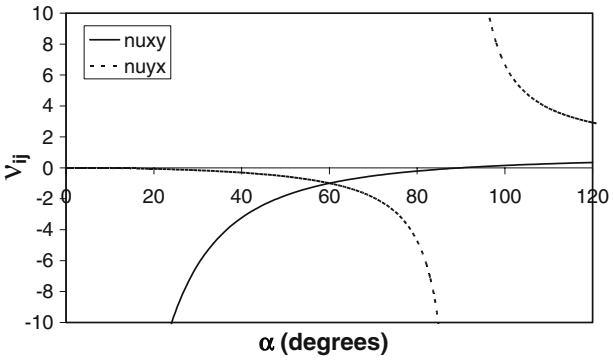

Fig. 5 Poisson's ratios as functions of α ($l_1 = l_2 = 1$; $a = 0.01$)

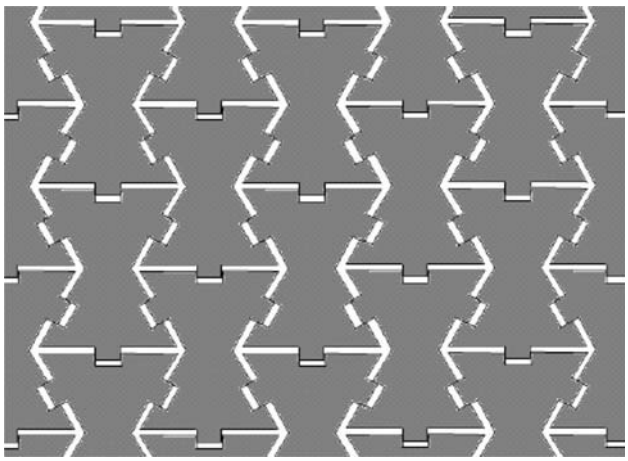

Fig. 6 Re-entrant interlocking hexagon structure

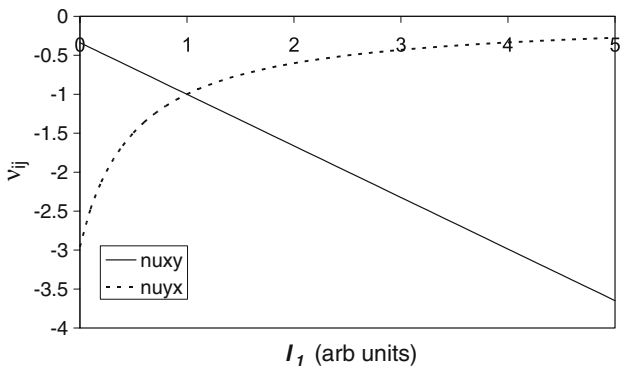

Fig. 7 Poisson's ratios as functions of edge length l_1 ($\alpha = 60°$; $l_2 = 1$; $a = 0.01$)

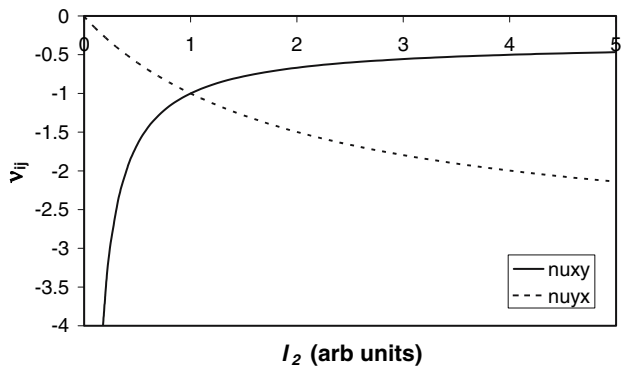

Fig. 8 Poisson's ratios as functions of edge length l_2 ($\alpha = 60°$; $l_1 = 1$; $a = 0.01$)

has a large negative value at $a = 0$ ($\nu_{xy} \sim -17$) and decreases in magnitude as a increases; ν_{yx} has a low negative value at $a = 0$ ($\nu_{yx} \sim -0.06$) and increases in magnitude as a increases.

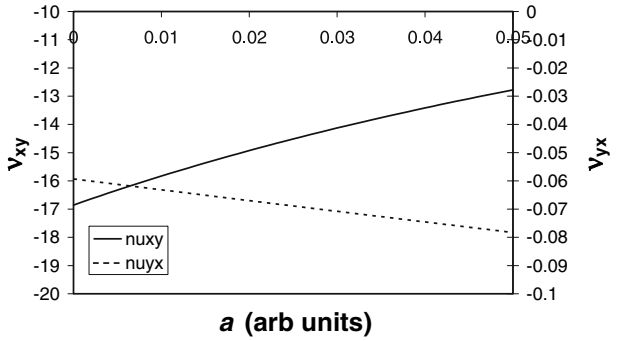

Fig. 9 Poisson's ratios as functions of gap parameter a ($\alpha = 30°$; $l_1 = 2$, $l_2 = 0.5$)

Young's modulus trends

Figures 10–13 show the dependencies of the Young's moduli on the geometrical parameters. In each case the Young's modulus has been normalised by the Young's modulus corresponding to the standard parameter set. In all cases the Young's moduli indicate highly anisotropic behaviour as the geometry changes away from the regular hexagon structure defined by the standard parameter set.

The Young's moduli show highly non-linear dependency on α (Fig. 10). E_x gradually decreases from infinity at $\alpha = 0°$ to a minimum at $\alpha = 100°$, before increasing slightly with α in the range $100 < \alpha \leq 120°$. E_y, on the other hand, shows a rapid decrease from infinity at $\alpha = 0°$ to a minimum at $\alpha = 6°$, before increasing back to infinity as $\alpha \rightarrow 90°$. Further increases in α in the range $90 < \alpha \leq 120°$ show a decrease in E_y.

E_x increases linearly with l_1 (Fig. 11) and decreases non-linearly with l_2 (Fig. 12), whereas E_y follows non-linear decreasing and increasing trends with l_1 and l_2, respectively (Figs. 11 and 12).

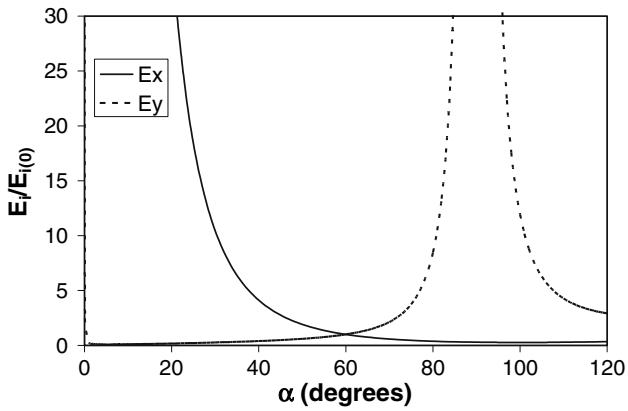

Fig. 10 Young's moduli as functions of α ($l_1 = l_2 = 1$; $a = 0.01$)

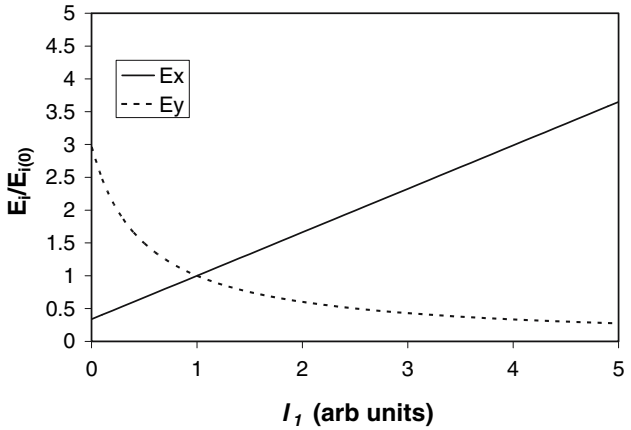

Fig. 11 Young's moduli as functions of edge length l_1 ($\alpha = 60°$; $l_2 = 1$; $a = 0.01$)

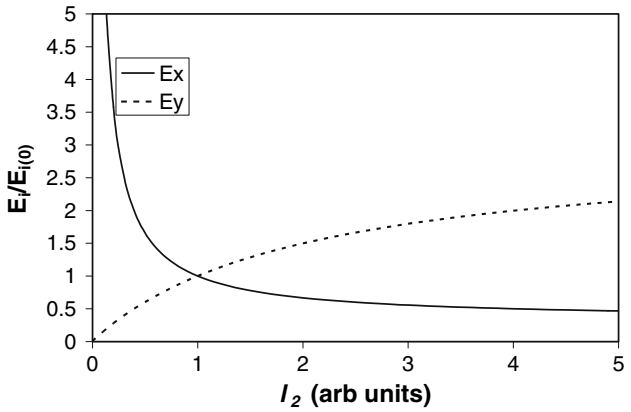

Fig. 12 Young's moduli as functions of edge length l_2 ($\alpha = 60°$; $l_1 = 1$; $a = 0.01$)

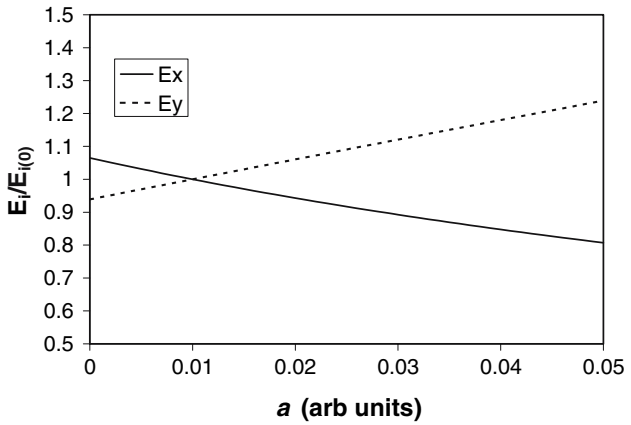

Fig. 13 Young's moduli as functions of gap parameter a ($\alpha = 30°$; $l_1 = 2$, $l_2 = 0.5$)

Similar to the case for the Poisson's ratios, the Young's moduli of the interlocking regular hexagon structure defined by the standard parameter set are independent of variation in a. However, for non-regular hexagon geometries, the Young's moduli show a dependency on a. For the example of hexagons having the non-standard parameter set of $\alpha = 30°$ $l_1 = 2$ and $l_2 = 0.5$, increasing a leads to a near-linear decrease in E_x and a linear increase in E_y (Fig. 13) in the range $0 \leq a \leq 0.05$.

Results—comparison of model predictions with experiment

The PP film experimental data [18] were employed in the comparison of the model predictions with experiment. This is due to the facts that mechanical properties data have been measured in both principal in-plane directions (whereas the fibre data are measured for loading along the length of the fibre only) and that the films are more homogeneous than the fibres.

The shape of the starting PP powder particles is known to typically approximate an elliptical cross-section rather than a circular cross-section [15]. The starting powder particles, therefore, have major and minor axes and in the following it is assumed the particle aspect ratio is maintained as surface melting occurs during the partial melt extrusion process to produce the fused/contacting particle microstructure of the auxetic film.

The choice of the alignment of the particle long axis with respect to the model axes (x and y) is arbitrary, as is the alignment of the model axes with the experimental extrusion direction. The extrusion direction is denoted by '∥' and the in-plane direction perpendicular to the extrusion direction by '⊥'. In order to illustrate the approach adopted to enable a comparison between model and experiment we consider, in the following, the case of the particle long axis aligned along the model x axis (i.e. long axis length = A) which is assumed to correspond to the extrusion direction of the film (i.e. model x axis corresponds to experimental '∥' axis). A fully densified structure ($a = 0$) is assumed, consistent with the observation of low porosity in the fibre/film microstructure (Fig. 1).

To determine the geometrical parameters of the particles to be employed in the model calculations parametric fits of the model expressions to the experimental values are performed for particle aspect ratio and the ratio of Young's moduli. Model predictions of the individual Poisson's ratios and Young's moduli are then evaluated for the derived model parameters.

Table 1 summarises the key experimental mechanical properties of the auxetic PP film and the geometrical parameters for the starting PP powder [15, 18].

Equating the ratio of Young's modulus in the extrusion direction with respect to that in the perpendicular direction

Table 1 Experimentally determined in-plane mechanical properties of auxetic PP films [18] and starting powder particle geometry [15] (|| = extrusion direction; ⊥ = perpendicular to extrusion direction)

$v_{\|}$	$v_{\perp}$	$E_{\|}$ (GPa)	$E_{\perp}$ (GPa)	Particle aspect ratio	Ave. particle size (μm)
–1.12± 0.06	–0.77± 0.01	0.34± 0.01	0.20± 0.01	1.87	52

$(E_{\|}/E_{\perp} = 1.7)$ to the interlocking hexagon model ratio (E_x/E_y) (Eqs. 21 and 22) when $a = 0$:

$$1.7 = \cos^2\alpha\left(\frac{l_1 + l_2\cos\alpha}{l_2\sin^2\alpha}\right)^2 \tag{26}$$

Similarly, equating the experimentally measured average starting powder particle aspect ratio (1.87) to the aspect ratio of the ellipse inscribed in the hexagon (Eq. 25):

$$1.87 = \frac{\sqrt{l_1^2 + 4l_1l_2\cos\alpha}}{2l_2\sin\alpha} \tag{27}$$

Solving Eqs. 26 and 27, we find,

$$\frac{l_1}{l_2} = 2.86 \tag{28}$$

$$\alpha = 69.2^\circ \tag{29}$$

Figure 14 shows the predicted strain in the y direction (ε_y) plotted against the predicted strain in the x direction (ε_x) for the above derived parameters (Eqs. 28 and 29). The strain in the x direction was calculated using the total true strain definition:

$$\varepsilon_x = \ln\left(\frac{X}{X_0}\right) \tag{30}$$

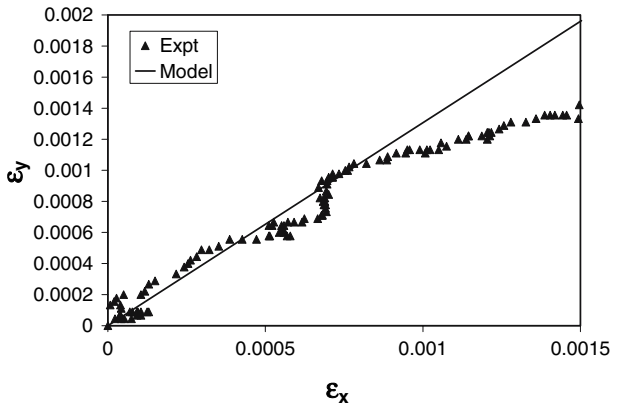

Fig. 14 Predicted model transverse total true strain (ε_y) versus axial total true strain (ε_x) for $\alpha = 69.2^\circ$; $l_1/l_2 = 2.86$, assuming an initially fully dense structure (i.e. $a = 0$ for the undeformed structure). Also shown, for comparison, are the experimental transverse versus axial (extrusion) total true strain data [18] (assuming the extrusion direction corresponds to the model x direction)

where X is defined by Eq. 1 and X_0 is the initial unit-cell length in the x direction (corresponding to an initial value of $a = 0$ for the fully densified structure). A similar expression was used for the strain in the y direction. For comparison, the experimental strain in the transverse direction versus the experimental strain in the axial (extrusion) direction for the PP film is also included in Fig. 14. The model curve provides an excellent fit to the experimental data in the low strain region. Substituting the derived geometrical parameters into Eqs. 6 and 7, the Poisson's ratios are predicted to be $v_{xy} = -1.30$ and $v_{yx} = -0.77$, which compare well with the experimental values of $v_{\|} = -1.12\pm 0.06$ and $v_{\perp} = -0.77 \pm 0.01$, as expected from the slope of the strain–strain data in Fig. 14.

For the comparison of experimental Young's moduli with model predictions, the following assumptions are made:

1. The stiffness of the spring connecting each male–female interlock combination is determined by the stiffness of the re-solidified polymer at the interface of 2 adjacent particles which have undergone simultaneous contact and surface melting during the extrusion process. The spring constant will, therefore, be determined to a first approximation from the Young's modulus of film extruded from fully molten PP polymer (i.e. at higher extrusion temperature) under otherwise similar process conditions to the auxetic film.
2. Particle depth in the model is equal to the average particle dimension measured experimentally (= 52 μm [15]).
3. The upper limit on the thickness of the partial melting interfacial region is equal to the average particle dimension (i.e. the maximum melt interface region corresponds to full melting of the particles).
4. Particles have perfectly bonded interface regions.
5. The unit-cell depth (in the out-of-plane z axis) is equal to the film thickness (~150 μm [18]). This is reasonable since there will be of the order of 3 starting powder particles (average dimension = 52μm) across the thickness of the film.

The stiffness constant k_h is defined as the ratio of the force F causing a change Δl_{int} in the thickness of the re-solidified melt interface region l_{int}:

$$k_h = \frac{F}{\Delta l_{\text{int}}} \tag{31}$$

It follows from Eq. 31 that the stiffness constant can be represented by,

$$k_h = \frac{E_{\text{int}} A_{\text{int}}}{l_{\text{int}}} \tag{32}$$

where E_{int} is the Young's modulus of the interface material and A_{int} is the average cross-section area of a face of the hexagon.

Considering the 6 faces of the hexagon, the average cross-sectional area A_{int} is given by,

$$A_{\text{int}} = \frac{(4l_2 + 2l_1)d}{6} \tag{33}$$

where d is the depth of the particle, assumed equal to the average size of the PP powder (= 52μm).

The assumption that E_{int} is given by the modulus of the conventional film produced using fully molten polymer during extrusion leads to E_{int} = 0.61GPa [18]. For the assumption that the upper limit on the thickness of the partial melting interfacial region is equal to the average particle dimension (i.e. l_{int} = 52μm), Eqs. 28, 32 and 33 give k_h = 19.1 kN/m. Assuming the depth of the unit cell (in the z direction) corresponds to the thickness of the auxetic PP film (= 150μ m) requires the Young's moduli expressions (Eqs. 21 and 22) of the interlocking hexagon model (which assume unit thickness along the z direction) to be modified by dividing them with this thickness factor. For the derived geometrical parameters of Eqs. 28 and 29, the final values for the Young's moduli are then found to be E_x = 0.63 GPa and E_y = 0.37 GPa, which are almost a factor of 2 higher than the experimental values of $E_{\|}$ = 0.34± 0.01 GPa and $E_{\perp} = 0.20 \pm 0.01$ GPa.

Table 2 summarises the derived geometrical parameters and predicted mechanical properties for the above scenario of particle long axis aligned along the model x axis which is assumed to correspond to the extrusion direction of the film. Table 2 also contains the derived parameters and predicted mechanical properties for the other 3 combinations of particle long axis alignment with the model principal directions and extrusion direction, using the above methodology. For all 4 cases considered, the predicted Poisson's ratios for loading along and transverse to the extrusion direction are equal to –1.30 and –0.77, respectively, and show very close agreement with the respective experimental values of –1.1 and –0.77.

However, the predicted model Young's moduli vary slightly depending on the particle alignment and model orientation with respect to the extrusion direction. In all cases the model predictions overestimate the experimental values. The closest fit to the experimental values is achieved for the particle long axis and extrusion direction both aligned along the model y direction (E_y = 0.60 GPa and E_x = 0.35 GPa, compared to $E_{\|}$ = 0.34 GPa and $E_{\perp} = 0.20$ GPa, respectively).

The value of l_{int} = 52 μm employed in the calculation of the Young's moduli in Table 2 is the upper limit and is unrealistic since at this point the particle–interface structure is essentially all interface material. The calculations for Young's moduli have been repeated, therefore, for an arbitrary value of l_{int} = 10.4 μm, corresponding to an interface thickness of 20% of the average particle dimension. The data are presented in Table 3 and show an in-

Table 2 Interlocking hexagon model parameters and predicted Poisson's ratios and Young's moduli

	Extrusion direction along x		Extrusion direction along y	
	Particle long axis along x	Particle long axis along y	Particle long axis along x	Particle long axis along y
Input parameters				
E_x/E_y	1.700	1.700	0.588	0.588
Aspect ratio (A/B)	1.87	0.535	1.87	0.535
Derived parameters				
l_1 (μm)	55.40	8.94	60.38	12.04
l_2 (μm)	19.38	48.34	18.54	41.67
α (°)	69.2	44.5	77.8	54.4
k_h (kN/m)	19.1	21.5	19.8	19.4
Predicted mechanical properties				
ν_{xy}	–1.30	–1.30	–0.77	–0.77
ν_{yx}	–0.77	–0.77	–1.30	–1.30
E_x (GPa)	0.63	0.75	0.54	0.35
E_y (GPa)	0.37	0.44	0.91	0.60

Calculations performed for thickness of interface region (l_{int}) = particle depth (d) = average particle dimension = 52μm and E_{int} = 0.61GPa

Table 3 Interlocking hexagon model parameters and predicted Young's moduli for l_{int} = 10.4 μm, particle depth (d) = average particle dimension = 52 μm and E_{int} = 0.61 GPa

	Extrusion direction along x		Extrusion direction along y	
	Particle long axis along x	Particle long axis along y	Particle long axis along x	Particle long axis along y
Input parameters				
E_x/E_y	1.700	1.700	0.588	0.588
Aspect ratio (A/B)	1.87	0.535	1.87	0.535
Derived parameter				
k_h (kN/m)	95.7	107.4	99.1	97.0
Predicted mechanical properties				
E_x (GPa)	3.14	3.77	2.67	1.76
E_y (GPa)	1.85	2.22	4.54	2.99

crease in the predicted Young's moduli as a result of the stiffness constant k_h increasing when the interface thickness decreases (Eq. 32). The model therefore consistently overestimates the Young's moduli.

Discussion

A model of a 2D network of interlocking rigid hexagons has been developed where deformation of the structure is via translation of the hexagons through sliding of adjacent hexagons along geometrically matched male–female interlock combinations. For the case of regular hexagons, the model is analogous to the geometry of the horizontal plane of existing 'keyed-brick' graphite structures at the macroscale and found in certain nuclear reactor cores. The model also has some similarity with rough particle (hard cyclic multimer) models developed to predict auxetic behaviour at the molecular level.

In particular, the hard cyclic trimer system with 3 small discs per multimer [41] maps onto the interlocking regular hexagon geometry. In this analogy, the curved contact between two adjacent small discs in the same trimer corresponds to a rectangular female interlock on the hexagon edge, whereas the curved contacts between one small disc in the trimer and two small discs in an adjacent trimer correspond to a rectangular male interlock on the hexagon edge.

In common with the macroscale keyed-brick structures and the molecular-level hard cyclic multimer systems, the interlocking hexagon model developed here is found to lead to auxetic behaviour. Bathurst and Rothenburg predicted a granular assembly could exhibit negative Poisson's behaviour when the tangential stiffness exceeds the normal contact stiffness between particles. The roughness of the particles appears to be the key in achieving this condition. In the model developed here the tangential stiffness approaches infinity for rigid hexagons with perfectly matched interlock combinations whereas the normal contact stiffness is finite and determined by the stiffness constant of the interlock spring. The interlocking hexagon model therefore satisfies the Bathurst and Rothenburg criterion for auxetic behaviour in a granular assembly.

The analytical expressions developed to predict the major Poisson's ratios and Young's moduli have been used to predict the effect of each of the parameters in the model on the mechanical properties of the interlocking hexagon structure (Figs. 5, 7–13). The ability to tailor the mechanical response of an interlocking hexagon structure through modifications to the geometry of the hexagons is clear from the parametric study. This includes the potential to design interlocking hexagon structures having extreme properties such as very large ('Giant') negative or positive Poisson's ratios ($|\nu_{ij}| \gg 1$) and large Young's moduli. The Poisson's ratios are determined purely by the geometrical parameters of the structure, whereas the Young's moduli also depend on the stiffness of the spring incorporated within each interlock combination. Interestingly, the model predicts positive Poisson's ratio behaviour when the hexagon angle exceeds 90° (Fig. 5), corresponding to a network of interlocking re-entrant hexagons (e.g. Fig. 6).

The model has been employed to predict the mechanical properties of PP films which derive their properties from structural features at the microscale. Appropriate geometrical parameters and spring constant were derived by fitting model expressions to known experimental values for the aspect ratio of the starting polymer powder and the ratio of the film Young's moduli. The experimental mechanical properties data for the auxetic PP film have been shown [18] to be consistent with the symmetric compliance matrix requirement from classical elasticity theory. The model has also been shown to satisfy the symmetric compliance matrix condition. Hence we would expect the ratio of the Poisson's ratio values to be predicted very well since this is equal to the ratio of the Young's moduli (Eq. 23).

The requirement that the strain energy of an orthotropic material be positive definite for static equilibrium leads to [40]

$$v_{ij} \leq \left(\frac{E_i}{E_j}\right)^{1/2} \tag{34}$$

For the experimental Young's moduli, Eq. 34 yields $|v_{\parallel}| \leq 1.30$ and $|v_{\perp}| \leq 0.77$. In the case of the model it has already been shown that $v_{xy} = v_{yx}^{-1}$ (Eq. 7). Employing the symmetric compliance matrix condition (Eq. 23) and the reciprocal relationship for the predicted in-plane Poisson's ratios for the model (Eq. 7) leads to predicted model Poisson's ratios having the maximum magnitude allowable according to Eq. 34 (i.e. equal to the square root of the ratio of the Young's moduli).

The experimentally measured values of $v_{\parallel} = -1.12 \pm 0.06$ and $v_{\perp} = -0.77 \pm 0.01$ are also close to the maximum magnitude allowable from strain energy considerations. However, there is no reciprocal relationship requirement for the 2 experimental in-plane Poisson's ratios and so Eq. 34 does not require the individual experimental Poisson's ratios to be equal to the maximum allowable values. Equation 34 merely provides the upper limit on the magnitude of the experimental values. The fact that the model predictions for the individual Poisson's ratios are in excellent agreement with the experimental values may, therefore, provide increased confidence that the mechanism for auxetic behaviour in the PP film is attributable to the translation of rough contacting/fused particles forming the film microstructure.

The predicted Young's moduli were consistently predicted to be higher than the experimental values. This may be attributable to the model geometry, fitting procedure and the additional assumptions that were required in the prediction of the Young's moduli values. These are briefly considered here.

As already noted, the method adopted to determine the geometrical parameters to employ in the model expressions comprised not only fitting the model ratio of the Young's moduli to the experimental Young's moduli ratio, but also fitting the aspect ratio of the inscribed ellipse in a hexagonal cell to the aspect ratio of the starting polymer powder. The aspect ratio fitting procedure has no impact on the Poisson's ratio predictions since this is purely determined by the Young's moduli ratio fit (see above—reciprocal relationship Eqs. 7 and 34). However, it does affect the individual Young's moduli. The choice of a hexagonal particle could, therefore, be one source of discrepancy, as could the assumption that the fused particles in the final film microstructure retain the aspect ratio of the starting powder particles (i.e. the aspect ratio remains constant before and after particle surface melting during processing). There is, therefore, a need to develop alternative interlocking particle geometries (e.g. quadrilateral particles) and to perform detailed microscopy of the structure of auxetic fibres and films produced using the partial melt extrusion process.

The model developed in this paper is a 2D model and so it was necessary to make an assumption relating to the depth of the unit-cell in the out-of-plane direction. In the absence of any evidence to the contrary it was assumed the unit-cell thickness is equal to the thickness of the auxetic PP film. The consideration of alternative particle geometries in a future study should, therefore, also consider 3D interlocking particle shapes to enable the extension of the 2D model developed in this work into a full 3D model. Similarly, the development of a 3D model will be informed by the proposed detailed microscopy study of the structure of the fibres and films to enable a more accurate definition of the appropriate unit-cell depth to be employed in the model.

Turning now to the interface region between fused particles, two arbitrary values for the thickness of the partial melting interfacial region have been employed in the calculations: the upper limit equal to the average particle dimension and also a thickness equal to 20% of the average particle dimension. The predicted Young's moduli for these 2 interface thicknesses differed by a factor of 5. Furthermore, it was assumed that the interfaces between adjacent particles are perfectly bonded, which may not be true in practice and will therefore lead to an overestimation of the predicted Young's moduli. More detailed information on the nature of the interface is, therefore, also required from the proposed microscopy study.

The predicted Young's moduli are also dependent on the stiffness constant of the interlock spring (Eqs. 21 and 22), which offers a further potential source of discrepancy. The spring constant was itself related to the Young's modulus of the interfacial region (Eq. 32) which was assumed to be equal to the Young's modulus of the film produced from fully molten PP polymer (i.e. processed at higher temperature) under otherwise similar processing conditions to the partial melt extruded films. At first sight this is reasonable since both films undergo similar (little) drawing during the extrusion process which might produce similar molecular arrangements in the melt phase and therefore similar Young's moduli. However, it is possible that local deformation of the interface material may be occurring during the extrusion process for the partial melt extruded films which could result in different molecular arrangements in the interface than occur in the bulk film produced at higher processing temperature. This would lead to different Young's moduli for the interface material in the partial melt extruded film than for the bulk full melt extruded film. Structural studies could usefully provide

information on the respective molecular arrangements from which to infer the veracity of the assumption of the interface Young's modulus employed in the calculation of the spring constant used in the fibre/film Young's modulus predictions.

Finally, defects in the film material may also account for some of the discrepancy between the predicted and experimental Young's moduli. An axial Young's modulus of 1.34 GPa has been reported for auxetic PP fibres [19], which is significantly higher than 0.34 GPa for the PP films produced under similar conditions. The fibre diameter is an order of magnitude smaller than the in-plane width of the films, leading to reduced potential for the presence of defects in the fibres and a correspondingly higher axial Young's modulus. The fibre axial Young's modulus is within the range of predicted values along the extrusion direction of 0.6–4.5 GPa for the various particle orientation, model axis alignment and interface thickness combinations considered in this paper (Tables 2 and 3).

Conclusions

A model of 2D interlocking rigid hexagons undergoing translation along the interlocks when subject to an applied load has been developed. The model geometry is consistent with SEM observation of a low porosity, fused or contacting particle microstructure in auxetic fibres and films produced from a partial melt extrusion process. Expressions for the in-plane Poisson's ratios and Young's moduli have been developed and a parametric study performed to demonstrate the potential to tailor the mechanical response of the rough hexagon assembly through careful selection of particle geometry and interlock spring constant. Interlocking hexagons having conventional hexagon geometry ($0 < \alpha < 90°$) lead to auxetic (negative Poisson's ratio) behaviour for the assembly, whereas re-entrant hexagons ($90 < \alpha < 180°$) lead to positive Poisson's ratio behaviour. Comparison of the model predictions with experimental Poisson's ratio data for auxetic PP films show very good agreement can be achieved. The predicted Young's moduli are consistently higher than the experimental values for the auxetic films, but are in reasonable agreement with the axial Young's modulus of the auxetic fibres.

Appendix: derivation of aspect ratio of inscribed ellipse within an hexagonal cell

The inscribed ellipse touches the hexagonal cell edges at S and P (Fig. 4). Taking the origin of the x–y co-ordinate system to be,

$$O \equiv (0, 0) \tag{A1}$$

the co-ordinates of the hexagonal cell corners Q and R are given by,

$$Q \equiv (l_1 + l_2 \cos\alpha, 0) \tag{A2}$$

$$R \equiv \left(\frac{l_1}{2}, l_2 \sin\alpha\right) \tag{A3}$$

The equation of the inscribed ellipse is given by,

$$\frac{x^2}{(A/2)^2} + \frac{y^2}{(B/2)^2} = 1 \tag{A4}$$

where, A and B are the axes of the ellipse aligned along the x and y axes, respectively.

The coordinates of P can be defined in parametric form as,

$$P \equiv \left(\frac{A}{2}\cos T, \frac{B}{2}\sin T\right) \tag{A5}$$

where, T is any arbitrary angle in space.

However, it is noted from Fig. 4 that B is equal to length SS'. Thus,

$$B = SS' = 2l_2 \sin\alpha \tag{A6}$$

It can be observed from Fig. 4 that the slope of the tangent to the ellipse at P is equal to the slope of RQ. Hence,

$$-\frac{B\cot T}{A} = -\tan\alpha \tag{A7}$$

Since the point P lies on the line QR, the slope of line RQ will be equal to the slope of QP. Thus,

$$-\tan\alpha = \frac{B\sin T}{A\cos T - l_1 - 2l_2\cos\alpha} \tag{A8}$$

Therefore, from Eqs. A6–A8, the aspect ratio of an ellipse inscribed in the hexagonal cell is,

$$\frac{A}{B} = \frac{1}{2l_2\sin\alpha}\sqrt{l_1^2 + 4l_1 l_2\cos\alpha} \tag{A9}$$

References

1. Evans KE, Nkansah MA, Hutchinson IJ, Rogers SC (1991) Nature 353:124
2. Gibson LJ, Ashby MF (1988) Cellular solids: structure and properties. Pergamon Press, Oxford

3. Lakes RS (1987) Science 235:1038
4. Alderson KL, Evans KE (1992) Polymer 33:4435
5. Pickles AP, Alderson KL, Evans KE (1996) Polym Eng Sci 36:636
6. Lees C, Vincent JEV, Hillerton JE (1991) Biomed Mater Eng 1:19
7. Yeganeh-Haeri Y, Weidner DJ, Parise JB (1992) Science 257:650
8. Alderson KL, Pickles AP, Neale PJ, Evans KE (1994) Acta Metall Mater 42:2261
9. Choi JB, Lakes RS (1996) Int J Fract 80:73
10. Alderson KL, Webber RS, Mohammed UF, Murphy E, Evans KE (1997) Appl Acoust 50:23
11. Evans KE (1990) Chem Ind 20:654
12. Caddock BD, Evans KE (1989) J Phys D: Appl Phys 22:1877
13. Alderson KL, Webber RS, Kettle AP, Evans KE (2005) Polym Eng Sci 45:568
14. Alderson KL, Alderson A, Webber RS, Evans KE (1998) J Mater Sci Lett 17:1415
15. Alderson KL, Alderson A, Smart G, Simkins VR, Davies PJ (2002) Plast Rubb Compos 31:344
16. Ravirala N, Alderson A, Alderson KL, Davies PJ (2005) Phys Stat Sol (b) 242:653
17. Ravirala N, Alderson KL, Davies PJ, Simkins VR, Alderson A (2006) Textile Res J 76:540
18. Ravirala N, Alderson A, Alderson KL, Davies PJ (2005) Polym Eng Sci 45:517
19. Simkins VR, Alderson A, Davies PJ, Alderson KL (2005) J Mater Sci 40:4355. DOI: 10.1007/s10853-005-2829-3
20. Evans KE, Alderson A (2000) Adv Mater 12:617
21. Moyers R (1992) US Patent No. 5108413
22. Stott PJ, Mitchell R, Alderson K, Alderson A (2000) Mater World 8:12
23. Alderson KL, Alderson A, Davies PJ, Smart G, Ravirala N, Simkins VR (2006) J Mater Sci (in press)
24. Alderson A, Evans KE (1995) J Mater Sci 30:3319. DOI: 10.1007/BF00349875
25. Alderson A, Evans KE (1997) J Mater Sci 32:2797. DOI: 10.1023/A:1018660130501
26. Bathurst RJ, Rothenburg L (1988) Int J Eng Sci 26:373
27. Wojciechowski KW (2004) In: Tokuyama M, Oppenheim I (eds) Slow dynamics of complex systems. AIP Proceedings
28. Grima JN, Jackson R, Alderson A, Evans KE (2000) Adv Mater 12(24):1912
29. Keskar NR, Chelikowsky JR (1992) Phys Rev B 46:1
30. Grima JN, Evans KE (2000) Chem Commun 1531
31. Grima JN, Evans KE (2000) J Mater Sci Lett 19:1563
32. Ishibashi Y, Iwata MJ (2000) Phys Soc Jpn 69:2702
33. Grima JN, Alderson A, Evans KE (2005) Phys Stat Sol (b) 242(3):561
34. Alderson A, Evans KE (2002) Phys Rev Lett 89(22):225503-1
35. Poulter DR (1963) The design of gas-cooled graphite-moderated reactors. Oxford University Press, London
36. Muto K, Bailey RW, Mitchell KL (1963) Proc Inst Mech Eng 177:155
37. Alderson KL, Alderson A, Evans KE (1997) J Strain Anal 32:201
38. Beatty MF, Stalnaker DO (1986) J Appl Mech 53:807
39. Prall D, Lakes RS (1997) Int J Mech Sci 39:305
40. Lempriere BM (1968) Am Inst Aeronaut Astronaut 6:2226
41. Wojciechowski KW (2003) J Phys A: Math Gen 36:11765